Lithium-Ion Batteries

International Edition: DOI: 10.1002/anie.201507632
German Edition: DOI: 10.1002/ange.201507632

Probing Dynamic Processes in Lithium-Ion Batteries by In Situ NMR Spectroscopy: Application to $Li_{1.08}Mn_{1.92}O_4$ Electrodes

*Lina Zhou, Michal Leskes, Tao Liu, and Clare P. Grey**

The push for increased vehicle electrification and the use of batteries on the grid requires significant improvements in the performance, cost, and safety of rechargeable batteries. This has driven world-wide research efforts to find alternative Li-ion electrode materials offering high energy density, high power, low cost, and electrochemical stability. Understanding how the electrode materials operate under realistic operating conditions is a critical part of this research activity. In situ techniques, such as X-ray diffraction (XRD) and X-ray absorption spectroscopy (XAS) probe structure and oxidation state, but do not probe lithium mobility directly, lithium diffusion being one important criterion for achieving high rates and thus high power batteries. Herein we show how the in situ NMR methodology can be adapted to probe Li mobility and the nature of electrode phase transformations in real time as the battery is cycled, even when the material under investigation is paramagnetic.

The spinel $Li_{1+z}Mn_{2-z}O_4$ ($0 \le z < 0.33$) has attracted substantial interest over the past few years and is now used commercially in high-power batteries.[1] $Li[Li_zMn_{2-z}]O_4$ has a three-dimensional (3D) structure formed by cubic closed packed oxygen ions, in which Li and Mn ions, along with excess Li ($0 < z < 0.33$), occupy tetrahedral 8a sites and octahedral 16d sites, respectively.[1a] This 3D Mn_2O_4 lattice provides tunnels for efficient lithium-ion diffusion. $Li_{1+z}Mn_{2-z}O_4$ can be deintercalated electrochemically to remove $1-3z$ Li, retaining the cubic Mn_2O_4 framework throughout.[1a,2] Given the importance of this high-rate material and this structure type in general, we use $Li_{1+z}Mn_{2-z}O_4$ to demonstrate our in situ metrology. To our knowledge, so far only one study was published on the microscopic Li mobility in pristine $Li[Li_{0.04}Mn_{1.96}]O_4$.[3] Herein we aim to gain further insight into the microscopic Li dynamics during the charge/discharge processes in the Li excess spinel, $Li_{1.08}Mn_{1.92}O_4$.

The use of NMR spectroscopy to measure Li^+ mobility[4] offers some advantages over other electrochemical techniques, such as galvanostatic intermittent titration technique (GITT), potentiostatic intermittent titration technique (PITT), electrochemical impedance spectroscopy (EIS), in probing atomic-level dynamic processes and not being affected by surface effects, grain boundaries, or crystallographic phase boundaries.[5] Ion dynamics can be investigated when hopping between sites occurs on a time scale comparable to or shorter than the size of the NMR interactions[6] and motional processes at different time scales can be studied. For example, chemical exchange processes between sites with different resonance frequencies (caused in this case by Fermi contact shifts) can be probed on a time scale of ms to µs, while relaxation rate constants (spin–lattice, T_1 and spin–spin relaxation, T_2) probe processes in a broader range of ns to ms.[7] In this study, the Li dynamics in the paramagnetic material $Li_{1.08}Mn_{1.92}O_4$ are explored by measuring the T_2, in situ (i.e., under operando conditions) on a working battery. In practice, a Hahn-echo experiment is used to measure T_2 and thus the signal decay monitored arises from a combination of the intrinsic T_2 relaxation and the NMR interactions that are not refocused by the echo pulse; the decay constant is, therefore, denoted as T_2'.[8] These T_2' changes provide an indirect measurement of motional processes on the timescale of ms to µs and allow the nature of the order–disorder transitions occurring in the electrode during battery cycling to be investigated. The analysis is further supported by ex situ ^{7}Li magic-angle-spinning (MAS) NMR of $Li_{1.08}Mn_{1.92}O_4$ at different states of charge (SOC).

The ex situ ^{7}Li MAS NMR spectra of $Li_{1.08}Mn_{1.92}O_4$ (Figure 1) contain very weak resonances at 717 and

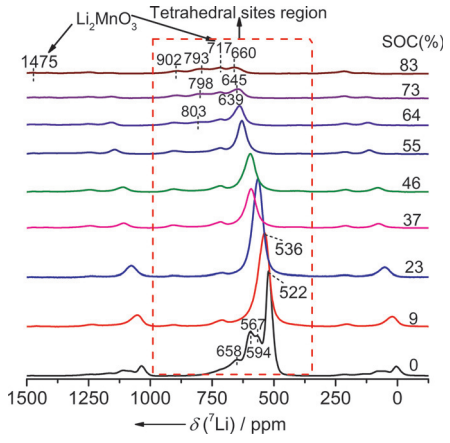

Figure 1. ^{7}Li MAS NMR spectra of $Li_{1.08}Mn_{1.92}O_4$ electrodes at different SOC. Spectra were acquired at 4.7 T with MAS frequency of 40 kHz. The resonances at $\delta = 1475$ and 717 ppm, marked on the spectra, arise from Li_2MnO_3. The isotropic shift regions are marked with a red dashed square; other spectral regions are dominated by the spinning sidebands. Spectra are normalized by the number of scan and the mass of the active material in the electrodes.

[*] Dr. L. Zhou, Dr. M. Leskes, Dr. T. Liu, Prof. C. P. Grey
Department of Chemistry
University of Cambridge
Lensfield Road, Cambridge CB2 1EW (UK)
E-mail: cpg27@cam.ac.uk
Homepage: http://www.ch.cam.ac.uk/person/cpg27
Dr. M. Leskes
Current Address: Department of Materials and interfaces
Weizmann Institute of Science (Israel)

Supporting information and ORCID(s) from the author(s) for this article are available on the WWW under http://dx.doi.org/10.1002/anie.201507632.

1475 ppm at all SOC because of trace Li_2MnO_3 impurities, their presence indicating that the Li content of the spinel sample is slightly lower than the nominal content 1.08 (1.08:1.92 Li:Mn). Interestingly, at the beginning of charge (9% SOC) the resonances between δ = 500–750 ppm, assigned to Li ions in tetrahedral sites,[3,9] collapse to a single broad resonance at δ = 536 ppm. This feature is indicative of motion on a timescale that is faster than the largest frequency separation (136 ppm; 10.5 kHz at 4.7 T) between the various resonances. Detailed two-site chemical exchange simulations using this frequency separation (Figure S4 in the Supporting Information) suggest a correlation time for Li hops between the tetrahedral 8a sites (h_{ex}) of the order of 40 μs. The increase in Li motion is facilitated by the Li vacancies, formed on charging. A second weak resonance at δ = 902 ppm appears at 9% SOC and remains upshifted until 83% SOC and is tentatively assigned to either an electrochemically formed double hexagonal (DH) phase[10] (see Supporting Information) and/or Li in tetrahedral sites near octahedral defects.[9b] The main resonance (at δ = 536 ppm at 9% SOC), assigned to Li in tetrahedral sites, continues to shift to high frequencies consistent with an increase in Mn average oxidation state, but remains as a single resonance up to 83% SOC, indicating that the rapid Li motion persists. A weak peak at δ = 803 ppm is observed at 64% SOC from a new Li^+ environment. As the SOC increases further, the main resonance now at δ = 639 ppm and the weak resonance at δ = 803 ppm shift slightly towards each other. This change suggests that Li chemical exchange (Li hopping) occurs between these sites, but on a slower time scale than the exchange between sites that gives rise to the major resonance at δ = 639 ppm (see Supporting Information for details). This slower exchange process is further confirmed by a two-dimensional chemical exchange experiment performed on $Li_{1.08}Mn_{1.92}O_4$ at 73% SOC (Figure S3). No exchange is seen between the δ = 639 and 803 ppm and the δ = 902 ppm resonances, consistent with the assignment of the δ = 902 ppm resonance to either a second (possibly, DH) phase or a more trapped Li environment. The δ = 803 ppm resonance is ascribed to Li^+ near octahedral Li^+ defects on the Mn sub lattice (see Supporting Information for further discussion of ^{7}Li MAS NMR shifts). In short, the ^{7}Li MAS NMR spectra suggest that Li chemical exchange is occurring between different Li sites throughout the charging process.

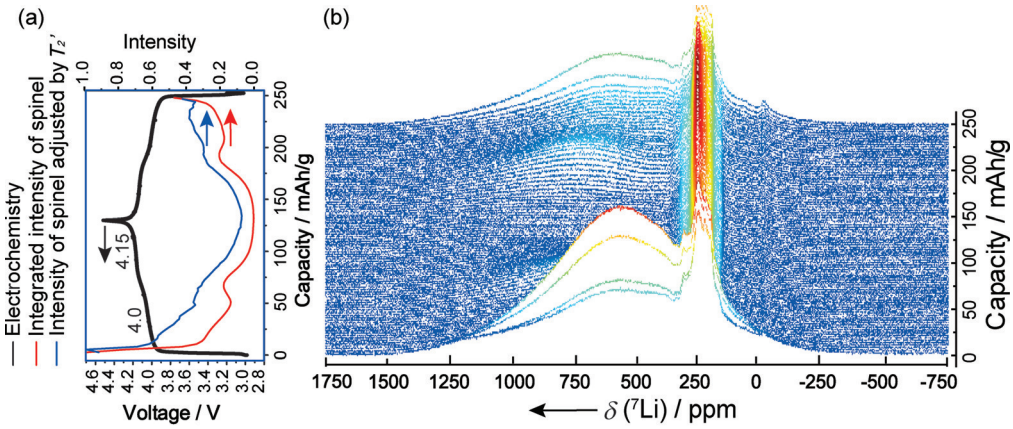

Figure 2. In situ ^{7}Li static NMR spectra for the first cycle of a $Li_{1.08}Mn_{1.92}O_4$ versus Li/Li^+ bag cell at 25 °C. a) Voltage profile (black), integrated intensity of the spinel resonance (red) and intensity of the spinel resonance (blue) adjusted by the corresponding in situ T_2' values (red triangles in Figure 3) versus capacity plots. b) ^{7}Li NMR stack plot. The in situ cell was cycled galvanostatically with a C/50 rate between 3.0 and 4.5 V during the spectra acquisition. A Hahn-echo pulse sequence (echo delay, 10 μs) was used to collect a total of 72000 scans for each spectrum, in approximately 60 min. The short recycle time (0.05 s) lead to suppression of the δ = 0 ppm electrolyte signal. Both the integrated intensity and the intensity adjusted by the corresponding in situ T_2' of the spinel are normalized to 1.

The removal of Li occurs by two processes at approximately 4.0 and 4.15 V (Figure 2a). The voltage step has been proposed to originate from Li ordering on the tetrahedral sub-lattice at 50% SOC,[1a,11] Li ordering resulting in a decrease in entropy and an increase in the free Gibbs energy of $Li_xMn_2O_4$, increasing the potential. Since the MAS spectra do not immediately provide insight into the nature of the two processes, in situ NMR spectroscopy was performed. The spectra are plotted as a function of capacity (where 128 $mAhg^{-1}$ corresponds to 100% SOC) in Figure 2. Since the in situ measurement is performed on a static sample, the various Li environments within the spinel electrode can no longer be resolved and only a single broad peak centered at δ = 560 ppm is observed. As described previously,[12] the battery was oriented so that the normal to the bag cell is at the magic angle, ensuring that bulk magnetic susceptibility shifts are minimized. As a result, the center of mass of the broad static resonance is close to the center of mass for the isotropic resonances observed when spinning. The resonance at about δ = 250 ppm arises from the Li metal anode. The spinel resonance shifts to high frequencies and decreases in intensity, as Li is removed from tetrahedral sites and Mn^{3+} is oxidized to Mn^{4+} during charging. During the discharge process, the trends in electrochemistry and shift in the spinel peak position are reversed, as expected.

Since the NMR signal depends linearly on the concentration of NMR active spins, a gradual, linear decrease in the intensity of the spinel signal with SOC might be expected. In contrast, a rapid decrease in Li intensity at the very beginning of charging is seen which is followed by an increase at 50% ("$Li_{0.5}$") and then a continued decrease until the end of the charge (red line, Figure 2a). The trend is reversed during on discharge. This deviation is ascribed to changes in the Li motion and thus to relaxation processes that occur during the Hahn echo evolution and refocusing times used in the acquisition of the NMR data. To confirm this, in situ T_2'

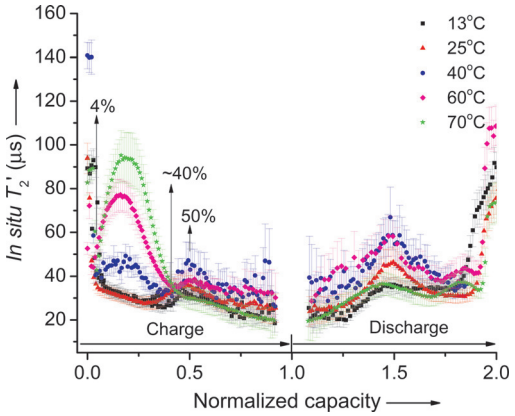

Figure 3. In situ ^{7}Li static T_2' Hahn echo measurements of $Li_{1.08}Mn_{1.92}O_4$ versus Li/Li^+ bag cells for the first cycle performed at 13 (black square), 25 (red triangles), 40 (blue circles), 60 (magenta diamonds), and 70 °C (green stars). The corresponding in situ T_2' values of the $Li_{1.08}Mn_{1.92}O_4$ electrode at different temperatures were plotted against normalized capacity, where 0 to 1 reflects the charge, and 1 to 2 reflects discharge (Li insertion). The capacity is normalized with respect to full capacity of $Li_{1.08}Mn_{1.92}O_4$. Black arrows indicate the corresponding SOC. Experimental details and the fitting protocols used to extract the T_2' values are given in the Supporting Information.

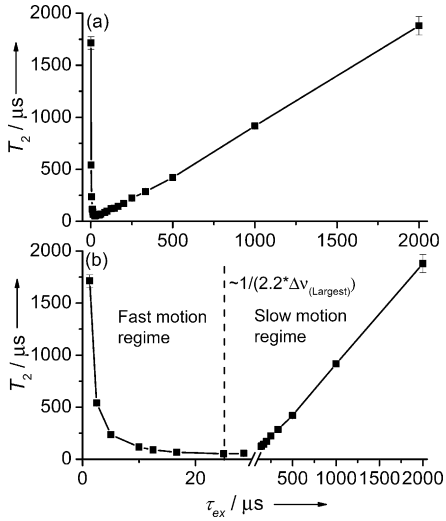

Figure 4. The plot of a) T_2 values versus the exchange time constant τ_{ex}. An expanded T_2 plot in b) showing that, on the left side of the curve, in the fast motion regime, T_2 is inversely proportional to the exchange time constant, τ_{ex}; on the right hand side, in the slow motion regime, T_2 is proportional to τ_{ex}. To illustrate the effect of motion on the T_2, simulations were performed for chemical exchange between 4 Li sites with the same frequency separation, $\Delta\nu$ (in units of Hz), as the four resonances for Li in tetrahedral sites in the pristine $Li_{1.08}Mn_{1.92}O_4$ sample (i.e., $\delta = 522, 567, 594, 658$ ppm (Figure 1) at a field strength of 7 T,). The simulated Hahn-echo decay curves for different values of τ_{ex} were then fit assuming a single exponential decay to extract the T_2 values.

values were measured for a second battery during cycling (Figure 3, 25 °C plot). The intensity of the spinel resonances were then corrected (blue line, Figure 2 a), by taking into account the signal decay during the echo period due to T_2' relaxation. A more gradual intensity decrease as Li is removed is now observed.

The initial rapid drop in T_2' (Figure 3) is correlated with the onset of rapid Li^+ motion, as observed by the coalescence of the different resonance in the ex situ ^{7}Li MAS NMR spectra (Figure 1). Simulations of the effect of multiple-site chemical exchange on the T_2 (Figure 4 and Figure S6a, S6b) confirm that a significant decrease in T_2 will occur when the Li hopping frequency is on the order of the frequency separation between the different Li resonances that contribute to the spectrum (i.e., in the kHz regime; see Supporting Information). In our simple model used herein to estimate the correlation times for Li^+ motions (τ_{ex}), that is, the exchange time for hops between different Li sites, we consider the effect of hops between sites that give rise to the four isotropic resonances of the pristine material MAS spectrum (Figure 1). The frequency shifts between resonances in a static spectrum are, in practice, a combination of different Fermi-contact shifts and/or Li-electron (Mn) dipolar interactions. After dropping further, the T_2' measured at 25 °C then increases noticeably as $Li_{0.5}$ (50 % SOC) is approached, which we ascribe to reduced Li motion, owing to the proposed Li ordering at this composition.[1a,11] This is consistent with the exhibition of a local minimum of the component diffusion coefficient D_j at $Li_{0.5}$ calculated by using Monte Carlo simulations based on the lattice gas model.[13] The T_2' decreases again as more Li is removed as Li vacancies are formed on the (partially) ordered $Li_{0.5}$ sub-lattice. Very little change in T_2' is observed above 60 % SOC.

As the temperature increases, similar overall features are observed in the in situ T_2' profile (Figure 3), although the phenomenon observed at 50 % SOC is less pronounced at higher temperature. This is ascribed to the increased Li motion and a suppression of the degree of Li ordering at $Li_{0.5}$ at higher temperatures. Of note, the T_2' between 4 and approximately 40 % SOC shows a strong dependence on temperature. A minimum in the T_2' (of ca. 25 µs) is observed at room temperature and below (at ca. 40 %). In contrast, the T_2' increases markedly between 4 and approximately 40 % SOC at higher temperatures, reaching a maximum at approximately 20 % SOC of 48, 76, and 93 µs at 40, 60, and 70 °C, respectively. As suggested by Figure 4, the increase in T_2' with increasing temperature provides compelling evidence that the Li motion at higher temperatures is now in the so-called fast motion regime, the regime where faster motion results in an increase in T_2.[14] The transition from slow to fast motion regime occurs when the Li hopping frequency is more than twice the largest frequency separation between different resonances, that is, when the correlation time for exchange is on the order of or less than 28 µs (Figure 4 and Supporting Information), within the simplified model used herein. Notably, the measured changes in T_2' on discharge during the 4.0 V process are very different from those seen on charge reflecting differences in the degree of ordering and structural pathways taken on charge and discharge (see Supporting Information for further discussion). Combined GITT and NMR experiments were performed in which the T_2' (and thus Li mobility) was measured during both the cycling and rest periods (Figure S7). Of note, the T_2' values measured from 8 to 40 % SOC were all systematically larger during charging

than during resting, reflecting faster Li^+ motion, presumably a consequence of a) increased disorder and b) the driven diffusional process. Further simulations are required to explore the driven diffusional proposal. At 4% SOC, the T_2' value measured on charging is lower than that measured during resting, supporting the proposal that motion at this SOC is still in the slow motional regime. Similarly at 44% SOC and above the motion returns the slow regime.

Many factors may in principle influence the measured T_2 values, including the electron relaxation times, T_{1e}, the rate of electron hopping between the Mn^{4+} and Mn^{3+} ions, and the Li motion. The longitudinal relaxation time, T_1, (which is mostly driven by high frequency processes) measured in a separate ex situ experiment decreases linearly upon charging and does not fluctuate in the same way as the T_2 (Figure S9). Additionally, the T_1 times are more than two orders of magnitude longer than the T_2 times. These observations suggest that high frequency motions are not the source of the T_2'. Both the electron relaxation, T_{1e} (usually 10^{-2}–10^{-7} μs[15]), and the electron hopping, (evaluated from the electronic conductivity data for $LiMn_2O_4$[16] to be approximately 10^{-1}–10^{-2} μs; see Supporting Information), correspond to high-frequency processes, indicating that, while these processes may be sources of T_1 relaxation, they are not the dominant sources of T_2 relaxation, that is, our T_2 measurements probe low-frequency motions, that is, Li dynamics. Future work involves the development of a global exchange model to take into account changes in the full ^{7}Li Hamiltonian on chemical exchange but is beyond the scope of this report.

Importantly, the smooth and non-linear variation of the T_2' with SOC, and its temperature behavior clearly shows that the electrode material is undergoing a solid–solution phase transformation between 0 and approximately 44% SOC (the 4.0 V process), consistent with in situ XRD measurements for related materials.[2,17] This observation does not rely on any understanding of the nature of the interactions that govern the T_2' relaxation mechanism, but follows from the fact that the signal decays measured in this regime cannot be fit by assuming a linear combination of two T_2' values from two end member phases. The nature of the structural phase transformation of the Li excess spinel above 50% SOC remains controversial and seems to depend on rate.[2,17] Our ex situ MAS results suggest that the regime between 64 and 83% SOC can be described at least locally in terms of a reaction between one component containing mobile Li ions and a second component containing more rigid Li ions nearer higher valent Mn ions. 2D exchange NMR experiments indicate that they are in close spatial proximity and not in two separate sets of particles. The changes in T_2' determined in situ do not vary noticeably from approximately 65 to 90% SOC (and 10–35% depth of discharge (DOD)) in this regime, and, as discussed in the Supporting Information, again resembling the behavior expected for a two phase reaction rather than a solid solution.

In conclusion, in situ T_2' relaxation measurements provide a simple method to monitor Li mobility during battery cycling, as a function of temperature. Since Li dynamics are strongly related to structural properties, the changes in in situ T_2' are used to indirectly detect structural changes, such as Li ordering. We expect this approach to be applicable in a wide range of battery systems where ion dynamics plays an important role in the battery's performance.

Experimental Section

Li excess spinel, $Li_{1.08}Mn_{1.92}O_4$ was synthesized by a solid-state method from Li_2CO_3 and Mn_2O_3. Li_2CO_3 (Fisher Scientific 99%) and Mn_2O_3 (Sigma Aldrich) were mixed in a Li/Mn ratio of 1.08/1.92, pelletized, and then heated at 650 °C for 12 h and 850 °C for 24 h.[9b,18] Heating and cooling rates were 2 °C min^{-1}. The $Li_{1.08}Mn_{1.92}O_4$ electrodes for ex situ MAS and in situ NMR experiments were prepared by mixing $Li_{1.08}Mn_{1.92}O_4$ powder, Super P Li (Timcal) with PVDF (Sigma Aldrich) in an 8:1:1 ratio, and 85% $Li_{1.08}Mn_{1.92}O_4$, 7.5% PTFE and 7.5% Super P Li, respectively. $Li_{1.08}Mn_{1.92}O_4$ vs. Li/Li^+ batteries were assembled in an argon glove box in either coin cells (for ex situ) or polyester plastic bag cells (for in situ) as described elsewhere.[9c,12] Electrochemical cycling of coin cells and in situ bag cells were carried out using an Arbin battery cycler and a Biologic VSP (Ultimate Electro-chemical Workstation), respectively. For ex situ NMR samples, the coin cells were charged to a certain SOC, and were then dissembled in the glove box and the active materials were extracted, washed, dried and packed into 1.8 mm diameter zirconia rotors for NMR measurements. NMR experiments were performed on 4.7 T Bruker Avance III 200, 7 T Tecmag LapNMR spectrometers.

Acknowledgements

This work was partially supported by the Assistant Secretary for Energy Efficiency and Renewable Energy, Office of Vehicle Technologies of the U.S. Department of Energy under Contract No. DE-AC02-05CH11231, under the Batteries for Advanced Transportation Technologies (BATT) Program subcontract no. 7057154. M.L. is an awardee of the Weizmann institute of Science—national postdoctoral award program for advancing women in science and a Marie Curie FP7 fellow.

Keywords: in situ spectroscopy · lithium-ion batteries · NMR spectroscopy · relaxation

How to cite: *Angew. Chem. Int. Ed.* **2015**, *54*, 14782–14786
Angew. Chem. **2015**, *127*, 14995–14999

[1] a) M. M. Thackeray, *Prog. Solid State Chem.* **1997**, *25*, 1–71; b) K. M. Shaju, P. G. Bruce, *Chem. Mater.* **2008**, *20*, 5557–5562.
[2] a) T. Ohzuku, M. Kitagawa, T. Hirai, *J. Electrochem. Soc.* **1990**, *137*, 769–775; b) X. Q. Yang, X. Sun, S. J. Lee, J. McBreen, S. Mukerjee, M. L. Daroux, X. K. Xing, *Electrochem. Solid-State Lett.* **1999**, *2*, 157–160.
[3] V. W. J. Verhoeven, I. M. de Schepper, G. Nachtegaal, A. P. M. Kentgens, E. M. Kelder, J. Schoonman, F. M. Mulder, *Phys. Rev. Lett.* **2001**, *86*, 4314–4317.
[4] a) W. Schmidt, P. Bottke, M. Sternad, P. Gollob, V. Hennige, *Chem. Mater.* **2015**, *27*, 1740–1750; b) A. Dunst, V. Epp, I. Hanzu, S. A. Freunberger, M. Wilkening, *Energy Environ. Sci.* **2014**, *7*, 2739–2752.
[5] M. Wagemaker, Interfacultair Reactor Institute Delft, Delft University of Technology (Netherlands), **2003**.
[6] A. Abragam, *Principles of Nuclear Magnetism*, Oxford University Press, **1961**, London.
[7] a) J. Cavanagh, W. J. Fairbrother, A. G. Palmer III, N. J. Skelton, *Protein NMR Spectroscopy: Principles and Practice*, Academic

Press, London, **1996**, pp. 243 – 300; b) D. Geschke, K. Poschel, *Colloid Polym. Sci.* **1986**, *264*, 482 – 487; c) R. Kimmich, *Makromol. Chem. Macromol. Symp.* **1990**, *34*, 237 – 248.
[8] G. B. Chavhan, *MRI Made Easy*, Jaypee Brothers Pvt. Ltd., New Delhi, **2013**.
[9] a) C. P. Grey, N. Dupré, *Chem. Rev.* **2004**, *104*, 4493 – 4512; b) Y. J. Lee, C. P. Grey, *J. Electrochem. Soc.* **2002**, *149*, A103 – A114; c) N. M. Trease, L. Zhou, H. J. Chang, B. Y. Zhu, C. P. Grey, *Solid State Nucl. Magn. Reson.* **2012**, *42*, 62 – 70.
[10] a) L. Dupont, M. Hervieu, G. Rousse, C. Masquelier, M. R. Palacín, Y. Chabre, J. M. Tarascon, *J. Solid State Chem.* **2000**, *155*, 394 – 408; b) M. R. Palacín, Y. Chabre, L. Dupont, M. Hervieu, P. Strobel, G. Rousse, C. Masquelier, M. Anne, G. G. Amatucci, J. M. Tarascon, *J. Electrochem. Soc.* **2000**, *147*, 845 – 853; c) M. R. Palacin, G. Rousse, M. Morcrette, L. Dupont, C. Masquelier, Y. Chabre, M. Hervieu, J. M. Tarascon, *J. Power Sources* **2001**, *97 – 98*, 398 – 401.
[11] J. B. Goodenough, M. M. Thackeray, W. I. F. David, P. G. Bruce, *Rev. Chim. Miner.* **1984**, *21*, 435.
[12] L. Zhou, M. Leskes, A. J. Ilott, N. M. Trease, C. P. Grey, *J. Magn. Reson.* **2013**, *234*, 44 – 57.
[13] S. W. Kim, S. I. Pyun, *Electrochim. Acta* **2001**, *46*, 987 – 997.
[14] a) J. A. Glasel, K. H. Lee, *J. Am. Chem. Soc.* **1974**, *96*, 970 – 978; b) C. Bonnet, P. H. Fries, S. Crouzy, P. Delangle, *J. Phys. Chem. B* **2010**, *114*, 8770 – 8781; c) R. A. Brooks, *Magn. Reson. Med.* **2002**, *47*, 388 – 391; d) R. Brooks, F. Moiny, P. Gillis, *Magn. Reson. Med.* **2001**, *45*, 1014 – 1020.
[15] G. Pintacuda, *Habilitation à diriger des recherches* thesis, Centre de RMN à Très Hauts Champs de Lyon (France), **2009**.
[16] M. Nishizawa, T. Ise, H. Koshika, T. Itoh, I. Uchida, *Chem. Mater.* **2000**, *12*, 1367 – 1371.
[17] a) M. Yoshio, H. Noguchi, H. Nakamura, K. Suzuoka, *Denki Kagaku* **1996**, *64*, 123 – 131; b) M. N. Richard, I. Koetschau, J. R. Dahn, *J. Electrochem. Soc.* **1997**, *144*, 554 – 557.
[18] Y. J. Lee, F. Wang, C. P. Grey, *J. Am. Chem. Soc.* **1998**, *120*, 12601 – 12613.

Received: August 14, 2015
Published online: October 12, 2015

